mathematics

Article

Estimating the Critical Velocity of the Incipient Motion of Particles on the Cuttings Bed Surface: An Experimental and Theoretical Analysis

Kaixiang Shen [1,2,*], Zhenqiang Xu [1,2], Guoshuai Ju [3,*], Yingsheng Wang [1,2] and Zijian Li [4]

1 Guangzhou Marine Geological Survey, China Geological Survey, Guangzhou 510075, China
2 National Engineering Research Center of Gas Hydrate Exploration and Development, Guangzhou 510075, China
3 College of Petroleum Engineering, Northeast Petroleum University, Daqing 163318, China
4 Department of Engineering and Applied Science, Memorial University of Newfoundland, St. John's, NF A1B 3X5, Canada
* Correspondence: skxv@163.com (K.S.); juguoshuai@nepu.edu.cn (G.J.)

Abstract: During the drilling of highly deviated and horizontal wells, a pump shutdown causes drill cuttings to settle and form a cuttings bed in the annulus. This study investigated the incipient motion law of the particles on the cuttings bed surface when the drilling fluid starts circulating again. This work could help field engineers to determine a reasonable incipient pump displacement to improve hole-cleaning efficiency. In this study, the effects of the well inclination angle, cuttings size, and different cuttings densities on the critical velocity of particle motion are analyzed experimentally, using a large-scale flow loop. Next, based on a stress analysis of the particles on the cutting bed surface and on the boundary layer flow around the particles, an analytical formula for the surface shear force of the drilling fluid on particles is derived and a critical velocity model for incipient motion is established. Verification is then carried out and combined with the experimental results. This study has important implications for the design of drilling operations and for the management of cuttings transport in oil and gas wells. It can guide the setting and prediction of pump discharge to improve hole-cleaning efficiency.

Keywords: cuttings bed; fluid mechanics; multiphase flows; incipient motion; deviated and horizontal wells

MSC: 76T25

check for updates

Citation: Shen, K.; Xu, Z.; Ju, G.; Wang, Y.; Li, Z. Estimating the Critical Velocity of the Incipient Motion of Particles on the Cuttings Bed Surface: An Experimental and Theoretical Analysis. *Mathematics* **2023**, *11*, 2689. https://doi.org/10.3390/math11122689

Academic Editors: Mingming Ge, Bin Ji and Desheng Zhang

Received: 4 May 2023
Revised: 4 June 2023
Accepted: 10 June 2023
Published: 13 June 2023

1. Introduction

A significant amount of drill cuttings are generated during the drilling of extended-reach and horizontal wells. These cuttings are removed from the wellbore by circulating drilling fluid to ensure that the wellbore is properly cleaned [1–3]. However, during the construction process, circulation must sometimes be stopped, for example, when changing a dull bit or making a connection, and then drill cuttings are deposited to form a cuttings bed. As the height of the cuttings bed increases, the drill pipe becomes buried. When circulation is restarted, the cutting particles on the cuttings bed surface are mobilized and transported to the wellhead by the drilling fluid. The inadequate removal of the cuttings bed can lead to hole cleaning problems such as high rotary torque, a stuck pipe, formation breakdown, a slow rate of penetration, and a loss of circulation [4–7]. Therefore, studying the incipient motion law of cuttings beds after the drilling fluid is recycled can guide field engineering practices in determining a reasonable pump displacement to improve hole-cleaning efficiency.

Currently, two types of theoretical models are used to describe cuttings transportation. One is the solid–liquid stratification model, which is based on theoretical assumptions and experimental observations, such as the two-layer model and the three-layer model [8–10].

This type of model can be used to calculate parameters such as the cuttings bed height and transportation efficiency. The other type of model calculates the critical velocity required for drilling fluid to carry and transport drill cuttings [11–13]. In order to inhibit the formation of a cuttings bed and to keep the wellbore's hole clean, the drilling fluid velocity needs to be greater than the critical velocity.

In terms of the stratification model, the two-layer model was initially established. However, the disadvantage of the two-layer model was that it did not consider the diffusion of particles from the bed surface to the liquid suspension layer. In their experiment, Nguyen and Rahman [14] observed that, at high flow rates, a mobile diffusion layer forms between the cuttings bed and the flow area of the drilling fluid. Therefore, based on the two-layer model, the mass and momentum balance equations of the mobile diffusion layer were added and a three-layer cuttings transport model was established. Kamp and Rivero [15] improved the solid phase concentration in the diffusion layer of the three-layer model by introducing the turbulence pulsation term, taking into account the promotion of turbulence in cuttings transportation. Cheng and Wang [16] divided the extended-reach well into three parts, where the horizontal and extended-reach well sections conformed to the characteristics of the three-layer model, and the moderately inclined well sections conformed to the characteristics of the two-layer model. The cuttings transportation in the vertical or near-vertical well sections only included the suspended layer. In addition to analyzing the control volume of the three-layer model, Ozbayoglu et al. [17] and Zhang et al. [18] also considered the influence of the force on the particles at the surface of the cuttings bed, making the three-layer model more complete. Wang et al. [19] solved the three-layer model using the SETS method and found that the cutting bed height and the drilling fluid displacement mutually affect each other, and that the well depth and displacement have a positive correlation with the cutting bed height. When the well depth reaches approximately 4000 m, the cutting bed height is no longer affected by the displacement and drill pipe rotation.

Regarding the incipient velocity model, when the velocity of the drilling fluid exceeds the critical velocity, the cuttings bed becomes unstable and continues to move forward. Compared to the two-layer and three-layer models, the incipient velocity model yields lower calculation values, providing a more pronounced advantage for parameter optimization. To ensure safe and efficient drilling, it is crucial to determine the incipient velocity accurately and reasonably. Clark and Bickham [20] conducted a force analysis on cutting particles at the bed surface, establishing the minimum transportation velocity (MTV) model. They identified three possible particle transportation states, including sliding, rolling, and lifting. Building on the MTV model, Ramadan et al. [21] considered the drag reduction effect of shear diluent liquid and introduced a downward plastic force, perpendicular to the flow direction of the force on the particles on the bed surface. The model results revealed that the rheological characteristics of the liquid phase also hindered particle start-up. Duan [11] incorporated the van der Waals force and used the near-bed velocity profile to establish an incipient velocity model for particles on the bed surface, accounting for factors such as particle size, rheology, and the inclination angle. Compared to other models, the incipient velocity model is easier to understand, providing a more direct guide for on-site engineers to optimize the discharge process. In recent years, in the field of fluid mechanics, machine learning methods have been used to process and analyze large amounts of experimental or simulated data to extract patterns or regularities related to the behavior of solid-liquid two-phase flows [22–24]. This combination can help researchers better understand and predict the characteristics of solid-liquid two-phase flows. In particular, GPU (Graphics Processing Unit) acceleration of machine learning has become a common method, which can significantly improve the speed of the training and inference processes. [25–27]

Currently, most incipient velocity models calculate the drag force based on the drag coefficient. However, there are numerous drag coefficient models available, which makes it challenging for field engineers to determine which model to use. This study analyzed the force applied to the particles on the surface of the cutting bed and the mechanism of the boundary layer flow to derive an analytical formula for the surface shear force of the drilling fluid's flow around the particles on the cutting bed. Thus, this study established a critical velocity model that considered the effects of the flow around the particles. The effects of the well inclination angle, the cuttings size, and the different cuttings densities on the critical velocity of particle motion were analyzed experimentally, using a large-scale flow loop. The findings in this study can offer guidance in setting and predicting pump discharge, which, ultimately, could improve the performance of hole cleaning.

2. Experimental Study

2.1. Experimental Setup

The experiment was based on the fluid–solid coupling experimental equipment for drilling fluid and drill cuttings. This equipment is crucial for developing a better understanding of the behavior of drilling fluid in a wellbore, which is essential for achieving efficient and effective drilling operations. The experimental setup consisted of a transparent acrylic pipe, which simulated the annulus of a horizontal well section, with a total length of 5.5 m. The inner wellbore diameter of the acrylic pipe was 120 mm, which is a standard size for many oil and gas wells. The outer diameter of the drill pipe was 73 mm, which, again, is a common size for the drilling equipment used in the industry (Figure 1).

Figure 1. Photograph of the critical velocity of particle motion experiment.

2.2. Test Materials

This study conducted experiments on the incipient velocity of drill cuttings using tap water and a poly aluminum chloride (PAC) solution. To prepare the PAC solution, this study mixed PAC powder with water and allowed the mixture to hydrate for a sufficient period. Prior to and after the experiments, the rheological properties of the test fluids were measured using an Anton Paar MCR92 advanced rheometer. The rheology of the PAC solution is best described by a power-law fluid model (k = 0.28 Pa.s^n, n = 0.65). The rheology of the tap water is best described by a Newtonian fluid model (μ = 0.0013 Pa.s). The solid phase of experiment consisted of glass and ceramic with different densities and particle sizes.

2.3. Experimental Setup

To accurately model incipient velocity, a stable cuttings bed with particles at a specific degree of subsidence and incipient motion is required. For deviated or horizontal well sections, the cuttings bed must be prepared in advance. Therefore, the incipient velocity measurement experiment was conducted as follows:

Step 1. Fluid and Particle Preparation: in this study, the shale shaker and recovery device were cleaned, then a specific concentration of experimental drilling fluid mother liquor was prepared before the experiment and it was stored it in the liquid storage tank for stirring and dilution. This study also added a sufficient quantity of experimental particles to the sand injection tank.

Step 2. Cuttings Bed Deposition: in this study, the sand-adding tank was opened to allow the experimental particles to enter the annulus using higher displacement. This created enough particles to form a stable cuttings bed. This study then reduced the displacement, kept the cuttings bed stationary and distributed the particles uniformly on the existing cuttings bed.

Step 3. Cuttings Bed Height Calculation: in this study, the displacement was reduced which made the particles static after sinking. Once a stable cuttings bed was formed, this study used protruding particles on the bed surface as the observation objects. Next, we took fixed-point photos and measured the bed height. Since the outer wall of the annulus is circular, the arc length was measured to obtain the corresponding cuttings bed height.

Step 4. Incipient Velocity Observation: in this study, we increased the flow rate of the drilling fluid by 0.004 m/s, until the observed particles on the bed surface started rolling and moving forward. To study particle motion on a bed surface, this study recorded the discharge required to initiate movement, reduced the discharge until the particles were stationary, and repeated the process.

During the incipient motion of a particle on the cuttings bed, a high-speed camera (Revealer 2F04C) was used to capture the incipient motion process at a frame rate of 100 frames/sec, as shown in Figure 2. The camera tracks particles using Lagrangian frames of reference. The observed particles on the bed surface first slowly rolled forward, then rolled slightly backwards, and, finally, continued to roll forward under the continuous drag of drilling fluid. These observations are depicted in Figure 2.

Figure 2. Schematic diagram of incipient motion of bed particles. (Red circle indicates observed particles).

3. Results and Analysis

3.1. Effect of Different Inclination Angles

The influence of the inclination angle on incipient velocity is illustrated in Figure 3. It is apparent from the figure that the incipient velocity was the highest in the wellbore sections with an inclination angle of 60–80°, making the incipient motion of drill cuttings particularly arduous.

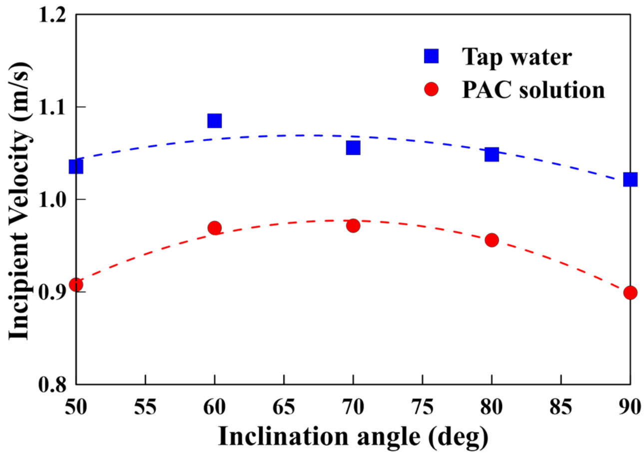

Figure 3. Influence of inclination angles on the incipient velocity of drill cuttings.

The analysis of the forces acting on the drill cuttings indicated that only the net weight force in the direction of the particle lifting was affected by the inclination angle, whereas all the other forces were independent of the wellbore inclination. Furthermore, the net weight force in the direction of the particle lifting increased with an increase in the wellbore inclination angle. In the horizontal wellbore sections, the drill cuttings were the least likely to be lifted and were primarily transported by a rolling mechanism. In the wellbore sections with a small inclination angle, the resistance force in the direction of the particle lifting was minimal, making the drill cuttings more prone to being lifted into the mainstream of the drilling fluid. In fact, in near-vertical wellbore sections, the gravitational force acting on the drill cuttings in the direction of settling towards the wellbore wall was entirely nullified, thereby fully entraining rock particles into the main flow.

3.2. Effect of Different Cuttings Sizes

The variations in the incipient velocity under different cutting size conditions are presented in Figure 4. The incipient velocity increased with the increase in the cutting sizes under two different drilling fluid conditions. The velocity required for the drill cuttings particles to move in the PAC experimental fluid was lower than that in the tap water experimental fluid. The specific pattern of the cuttings movement tended to remain constant within a smaller range of particle sizes, e.g., within the range of 1.0–2.0, and increased rapidly when the particle size exceeded a certain value.

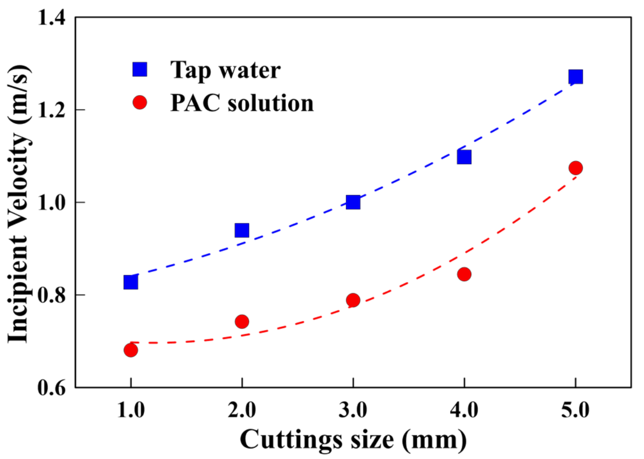

Figure 4. Influence of cuttings sizes on the incipient velocity of drill cuttings.

This phenomenon can be explained by analyzing the changes in the inertial forces concerning particle size. On the surface of the cuttings bed, the drag force of the drilling fluid caused the particles to start moving. When the particle size was small, the inertial force was greater than the shear stress applied to the particles and the movement of the particles on the surface of the cuttings bed tended to be stable. However, when the particle size exceeded a certain threshold, the inertial force experienced by the moving particles was smaller than the drag force of the drilling fluid, which made the effect of the particle size on the movement velocity more pronounced.

3.3. Effect of Different Cuttings Densities

The influence of the cuttings density on the incipient velocity is illustrated in Figure 5. When the particles on the surface of the cuttings bed were mobilized, the required flow rate of the drilling fluid increased with the density of the particles. The velocity required for the mobilization of the cuttings particles in the PAC experimental fluid was lower than that in the tap water experimental fluid. Increasing the density of the cuttings had a negative impact on their mobilization, leading to an increase in the height of the cuttings bed and a decrease in the effectiveness of the cleaning in the annular space.

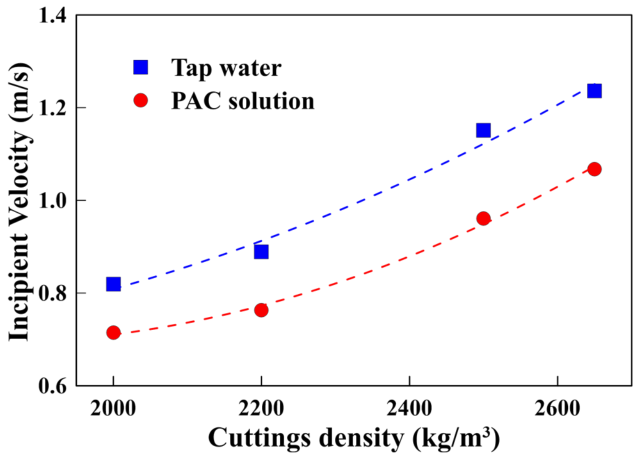

Figure 5. Influence of cuttings densities on the incipient velocity of drill cuttings.

The incipient velocity of drill cuttings increased with the increase in their density. The reason for this was that, as the density of the cuttings increased, the mass of the individual drill cuttings also increased, even though the volume remained the same. As a result, the energy required for the drill cuttings to start moving from a static state also increased, along with the incipient velocity. Due to the increase in the cuttings density, the decrease in the particle buoyancy, and the increase in the submerged weight, the average flow rate for the drilling fluid required for incipient velocity increased.

4. Model Development and Analysis

In this study, the following assumptions were made before establishing the incipient velocity model: (1) the drilling fluid is an incompressible medium; (2) spheres replace the actual irregular cutting particles with the same diameter; (3) the average bed surface replaces the actual cutting bed surface; and (4) the annulus is concentric, and the drill pipe does not rotate. Based on these assumptions, the incipient motion of the cutting particles on the bed surface was analyzed and the model was derived.

4.1. Shear Force of Flow around Cutting Particles on Cuttings Bed Surface

Due to the wellbore and the drill pipe forming a double-wall annular space, there was a velocity gradient distribution present in both the drill pipe and the wellbore. The effect of this velocity gradient distribution on particles can be simplified as the effect of different velocity layers on the particle.

The main force that moves particles on the cuttings bed surface is the drag force of the drilling fluid's flow along the flow direction. Since the annular space formed by the wellbore and the drill pipe had two walls, the annular drilling fluid had dual velocity gradient distribution characteristics. As shown in Figure 6, there was a maximum velocity on the annular surface, with a certain radius of the annulus.

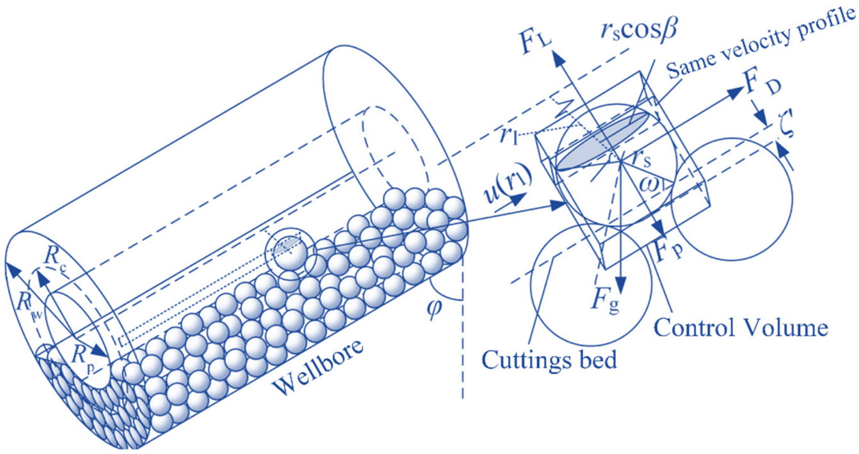

Figure 6. Geometric relationship of the control volume of drill cuttings bed surface in the annulus.

Assuming that the radius, R_c, corresponds to the maximum velocity of the annular surface, it can be calculated using the following expression:

$$R_c = \left(R_p + R_w \left(\frac{R_p}{R_w} \right)^{7/20} \right) \Big/ \left(1 + \left(\frac{R_p}{R_w} \right)^{7/20} \right) \tag{1}$$

where R_p is the drill pipe radius and R_w is the wellbore radius.

The exposure level, ζ, was introduced to define the degree to which a particle was exposed to the flow:

$$\zeta = \frac{\zeta'}{r_s} \tag{2}$$

where ζ' is the distance from the lowest point of the particles to the average bed surface; r_s is the average radius of the drill cuttings.

As shown in Figure 7, the calculation point was selected along the circumference as the origin to establish a Cartesian coordinate system. The potential flow velocity distribution around the circumference of the volume element was as follows:

$$U(\alpha) = 2u(r_1)\sin\alpha \tag{3}$$

where $u(r_1)$ is the corresponding mainstream velocity of each layer's volume element; r_1 is the distance from the particle center to the central axis.

The maximum flow velocity, u_{max}, in the annulus can be expressed as follows:

$$u_{max} = \overline{u} + \int_{R_p}^{R_c} u_1(r)dr + \int_{R_c}^{R_w} u_2(r)dr \tag{4}$$

where u_{max} is the maximum flow velocity in the annulus; $\overline{u}$ is the average flow velocity above the bed surface, which can be calculated as the ratio of the volume flow rate of the flow area above the bed surface to the flow-section area; $u_1(r)$ is the velocity distribution from the drill pipe to the maximum velocity annular surface; and $u_2(r)$ is the velocity distribution from the maximum velocity annular surface to the wellbore.

The expression for the velocity distribution in the annulus can be summarized as follows:

$$u_i(r_1) = u_{max} + \frac{u_{*i}}{2\kappa}\left(\frac{R_c - r_1}{\Delta R}\right) + \frac{u_{*i}}{2\kappa}\left(\frac{r_s}{\Delta R}\right)\cos\beta \tag{5}$$

where κ is the Karman constant, with κ = 0.41 when the velocity is distributed between R_p and R_c (i.e., i = 1, $\Delta R = R_c - R_p$), and when the velocity distribution is between R_c and R_w

(i.e., i = 2, $\Delta R = R_w - R_c$); u_* is the friction velocity, $u_* = \sqrt{\tau/\rho}$; u_{*1} is the friction velocity on the outer wall of the drill pipe; and u_{*2} is the friction velocity on the inner wall of the wellbore.

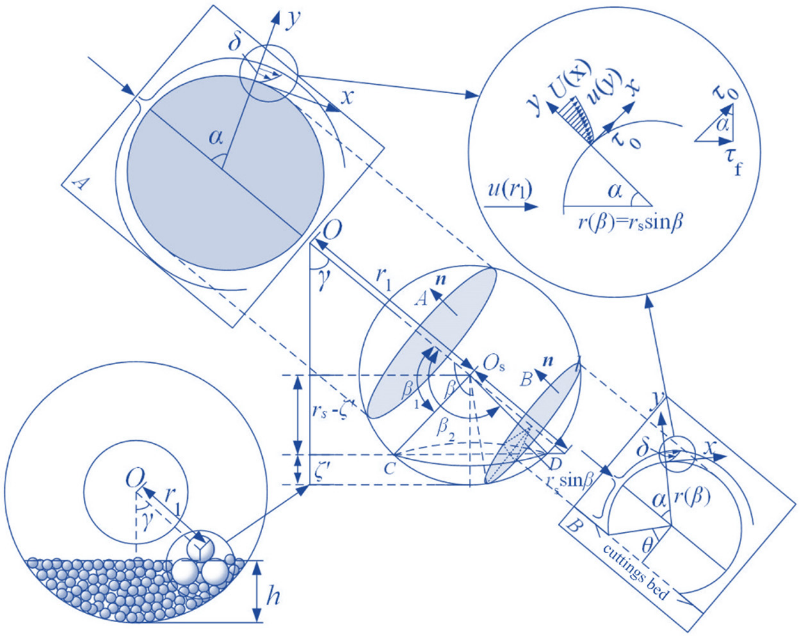

Figure 7. Cuttings particles incipient motion at different positions on the cuttings bed surface.

The surface shear force can be expressed as follows:

$$\tau = 0.5 f_f \rho \overline{u}^2 \tag{6}$$

where f_f is the average friction coefficient of the liquid flow [28], which can be calculated as follows:

$$\frac{1}{\sqrt{f_f}} = -2\lg\left(\frac{\varepsilon}{3.72D_h} + \frac{2.51}{\mathrm{Re}\sqrt{f_f}}\right) \tag{7}$$

where ε is the surface average roughness; D_h is the effective hydraulic diameter; and Re is the Reynolds number.

Let us suppose that the velocity distribution at the calculation point and the vertical height, y, from the particle surface meets $u(y) = ay^2 + by + c$, and that the boundary conditions are met as follows:

$$\begin{array}{l} y = 0,\ u(y)|_0 = 0 \\ y = \delta,\ u(y)|_\delta = U(\alpha),\ \frac{\partial u(y)}{\partial y}|_\delta = 0 \end{array} \tag{8}$$

According to the simplification of the integral equation, in this study we obtained the following:

$$\frac{u(r_1)}{5\nu r_\beta}\left(3\delta^2\cos\alpha + \frac{2}{3}\delta\delta'\sin\alpha\right) = 1 \tag{9}$$

where r_β is the radius of the corresponding area element of β; v is the fluid kinematic viscosity; δ is the boundary layer thickness for the flow around the particle; and δ' represents the derivative of the boundary layer thickness, with respect to radian α.

The fluid kinematic viscosity was calculated according to the following formula:

$$\nu = \frac{K}{\rho}\left[\frac{(2n+1)(R_w - R_p)}{18n\overline{u}}\right]^{1-n} \tag{10}$$

where n is the flow index and K is the consistency coefficient.

The boundary layer thickness, $\delta(\alpha)$, can be calculated as follows:

$$\delta(\alpha) = \sqrt{\frac{bC - 2\cos\alpha \cdot Hypergeometric_2F_1\left[\frac{1}{2}, -\frac{7}{2}; \frac{3}{2}; \cos^2\alpha\right]}{b\sin^9\alpha}} \tag{11}$$

where $Hypergeometric_2F_1\left[\frac{1}{2}, -\frac{7}{2}; \frac{3}{2}; \cos^2\alpha\right]$ is a Gaussian hypergeometric function, which is expanded by series. When determining the constant C, it is assumed that the initial boundary layer thickness, δ_0, starts to develop from the front stagnation point, α_0, as follows:

$$\delta_0 = \sqrt{\frac{0.00655864}{b\sin^9\alpha_0}} \tag{12}$$

Based on this assumption, in this study we obtained the following:

$$\delta = \sqrt{\frac{0.859 - \left(2\cos\alpha - \frac{7}{3}\cos^3\alpha + \frac{7}{4}\cos^5\alpha - \frac{5}{8}\cos^7\alpha\right)}{b\sin^9\alpha}} \tag{13}$$

In the above formula, $b = \frac{2u(r_1)}{15vr_\beta}$.

The shear force acting on any point around the circumference of the element is as follows:

$$\tau_0 = \frac{2\nu\rho U(\alpha)}{\delta} = \sqrt{\frac{(2\nu\rho \cdot 2u(r_1)\sin\alpha)^2 b\sin^9\alpha}{0.859 - \left(2\cos\alpha - \frac{7}{3}\cos^3\alpha + \frac{7}{4}\cos^5\alpha - \frac{5}{8}\cos^7\alpha\right)}} \tag{14}$$

The total shear force, $F_{\tau a}$, is obtained by integrating the shear stress along the undivided circumference and then along the axis, l.

$$F_{\tau\alpha} = 16\rho\sqrt{\frac{vr_s^3}{15}}\left(\int_0^\pi \sqrt{\sin\beta}u^{\frac{3}{2}}(r_1) \cdot 2F(\alpha)|_0^{\frac{9\pi}{20}} d\beta - \int_{\beta_1}^{\beta_2} \sqrt{\sin\beta}u^{\frac{3}{2}}(r_1) \cdot F(\alpha)|_{\frac{\pi}{2}-\theta}^{\frac{9\pi}{20}} d\beta\right) \tag{15}$$

The function, $F(\alpha)$, is obtained by the regression of the integral upper limit function and the integral value, as follows:

$$F(a) = -0.1359a^3 + 1.0201a^2 - 0.5179a + 0.0426 \tag{16}$$

where θ is the included angle between the line from the particle exposure point to the particle center and the vertical direction.

β_1 and β_2 meet the following requirements:

$$\begin{aligned} \beta_1 &= \pi - r - \arccos\tfrac{r_s - \zeta'}{r_s} \\ \beta_2 &= \pi - \gamma + \arccos\tfrac{r_s - \zeta'}{r_s} \end{aligned} \tag{17}$$

where γ is the position angle of the particles on the bed surface, as shown in Figure 2.

The particles on the bed surface are affected by both the annulus velocity gradient and also by the internal shear force of the viscous sublayer, which is expressed as $F_{\tau b}$. As shown in Figure 8, the volume differential element, C, was integrated from the outer boundary of the viscous sublayer to the inner boundary, and the boundary layer thickness can be expressed as follows:

$$\delta_p = 5u_*^{\frac{n-2}{n}}\left(\frac{K}{\rho}\right)^{\frac{1}{n}} \tag{18}$$

$$\tau_b = 0.5f_b\rho\overline{u}^2 \tag{19}$$

$$u_* = \sqrt{\tau_b/\rho} \tag{20}$$

where f_b is the average friction coefficient of the bed surface; τ_b is the average shear stress of bed surface; and δ_p is the bed boundary layer thickness.

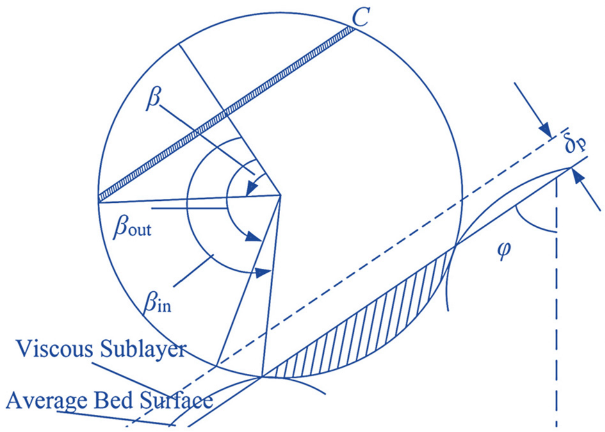

Figure 8. Geometric relationship for boundary layer of flow around the particles on the bed surface.

At the same time:

$$\begin{cases} \beta_{out} = \arccos(1-\zeta-\delta_p/r_s) \\ \beta_{in} = \arccos(1-\zeta) \end{cases} \tag{21}$$

where β_{out} is the outer boundary angle of the viscous sublayer integral, which refers to the angle from the top to the outer boundary of the viscous sublayer; and β_{in} is the integral internal boundary angle of the viscous sublayer, which is the angle from the top of the particle to the contact point with the average bed surface.

The velocity distribution inside the viscous sublayer is expressed as follows:

$$u_{in} = \frac{u_*^2}{v} r_s((1-\zeta)+\cos\beta) \tag{22}$$

The integral expression can be calculated as follows:

$$F_{\tau_b} = 8\rho\sqrt{\frac{2vr_s^3}{15}} \int_{\beta_{out}}^{\beta_{in}} \left(u_i^3 \sin\beta\right)^{0.5} F(a)\Big|_0^{\frac{9\pi}{20}} d\beta \tag{23}$$

The total surface shear force along the flow direction, F_τ, was obtained from the superposition of the shear force of the viscous sublayer's internal bed boundary layer and the external annulus's surface shear force, as follows:

$$F_\tau = F_{\tau a} + F_{\tau b} \tag{24}$$

4.2. Lifting Force of Bed Particles

The particles are also subject to a lifting force when the drilling fluid flows through the surface of the cuttings bed. The method for calculating the velocity, u_d, varies with the deposition degree of the cuttings bed.

When the deposition of the drill cuttings was dense and the flow was laminar, the linear Darcy's law was used for the calculation, as follows.

$$u_d = -\frac{\Delta p K_p}{\mu L} \tag{25}$$

where K_p is the permeability coefficient of the cutting bed; $\Delta p/L$ is the pressure drop gradient in the L measuring section; and μ is the dynamic viscosity of the drilling fluid.

When the drill cuttings deposition is non-dense, non-Darcy's law applies, as follows:

$$-\frac{\Delta p}{L} = \frac{\mu}{K_p} u_d + \beta_D \rho u_d^2 \tag{26}$$

where β_D is the non-Darcy factor, which can be calculated as follows:

$$\beta_D = \frac{1.59 \times 10^5}{q^{5.5}\sqrt{K_p}} \tag{27}$$

where q is the average porosity of the cuttings bed and K_p is the porous media permeability, which can be expressed as follows:

$$K_p = c_0 \frac{q^3}{(1-q)^2 M_s^2} \tag{28}$$

where C_0 is the coefficient (taking C_0 = 0.2); M_s is the specific surface area of the particles (for spherical particles, $M_s = 3/r_s$).

According to Bernoulli's principle, the lifting force and the average flow velocity on the bed surface, $\overline{u}$, as well as the flow velocity inside the bed, u_d, are related as follows:

$$F_L = 0.5\rho A_s \left(\overline{u}^2 - u_d^2\right) \tag{29}$$

where Δp_s is the difference between the upper and lower pressures of the particles; and A_s is the projected area of the particles that are perpendicular to the liquid flow direction.

4.3. Interaction Force between Bed Particles

There was also an adhesive force between particles, which is expressed as follows:

$$F_p = 2\left(\frac{5}{3}\right)^m \xi_s j^m r_s \tag{30}$$

where $\xi_s = 4.744 \times 10^{-6}$ kg/m, m = 10.

With respect to the ratio, j, of the dry volume weight and the volume weight, its expression is as follows:

$$j = \begin{cases} 0.52\left(\frac{r_s}{r_s+2\delta_s}\right)^3 & r_s \le 0.5 \text{ mm} \\ 0.70 - 0.18\exp\left(-0.095\frac{r_s-r_0}{r_0}\right) & r_s > 0.5 \text{ mm} \end{cases} \tag{31}$$

where δ_s is the thickness of the film water on the particles' surface, δ_s = 0.4 µm; and r_0 is the reference particles' radius, r_0 = 0.5 mm.

4.4. Incipient Velocity Calculation Process

First, this study determined the surface friction, F_τ, between the particles and the bed surface; the lifting force, F_L; and the interaction force, F_p, between the particles. Then, this study determined the incipient velocity required for the particles to start rolling, according to the condition that the total positive torque was greater than or equal to the total negative torque.

As shown in Figure 9, for highly deviated and horizontal well sections, the conditions for the particle rolling to start are as follows:

$$(F_{\tau a} + F_{\tau b})L_1 + (F_L - F_P)L_2 - F_g L_3 > 0 \tag{32}$$

$$L_1 = r_s(1-\zeta) \tag{33}$$

$$L_2 = r_s \sin[\arccos(1-\zeta)] \tag{34}$$

$$L_3 = r_s \cos[\varphi - \arccos(1-\zeta)] \tag{35}$$

where φ is the well deviation angle; F_g is the floating weight of the particles in the drilling fluid, as follows:

$$F_g = \frac{4}{3}\pi r_s^3(\rho_s - \rho)g \tag{36}$$

where ρ_s is the average density of the drill cuttings.

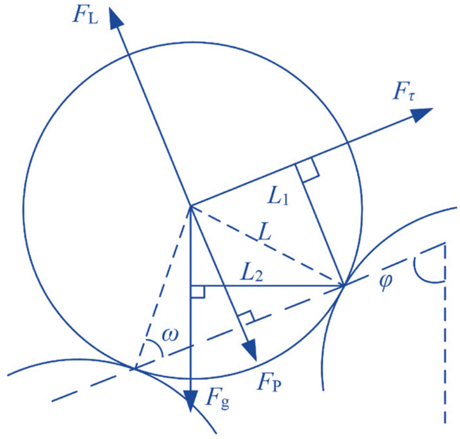

Figure 9. Schematic diagram of bed particles in the incipient state.

The calculation steps for determining the incipient velocity are depicted in Figure 10. The surface friction was computed based on the corresponding integral value. Next, the calculations of the lifting force, inter-particle interaction force, and other relevant factors were conducted. The iterative calculation of the average velocity continued until the critical rolling motion conditions were met, after which the velocity was deemed the incipient velocity, u_c.

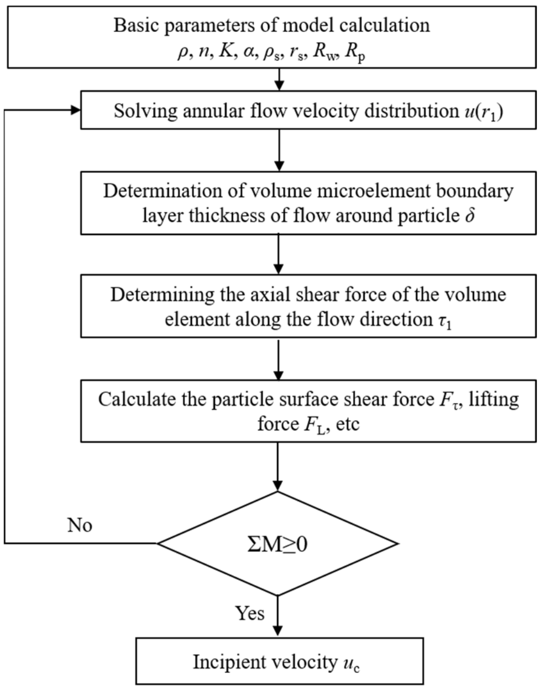

Figure 10. Calculation flow chart for incipient velocity of bed particles.

4.5. Measured and Predicted Initial Velocity

In this paper, in addition to predicting the critical velocity of the particles on the cuttings bed surface through theoretical derivation, it was also necessary to compare and analyze the incipient velocity predicted by the model with the experimental measurement data. The comparison between the model's prediction results and the experimental measurement results under three operating conditions is shown in Figure 11. As shown in Figure 11, the maximum relative deviation between the simulation and experimental results did not exceed 20%. This proves that the model established was relatively accurate and will be able to further simulate the incipient velocity under variable operating conditions. In addition, the relative error with the small velocity was relatively large, while the error after that was small. This was because the fluid field in the annulus underwent significant changes during the initial motion with small-circulated velocity. This error will decrease when the circulated velocity stabilizes.

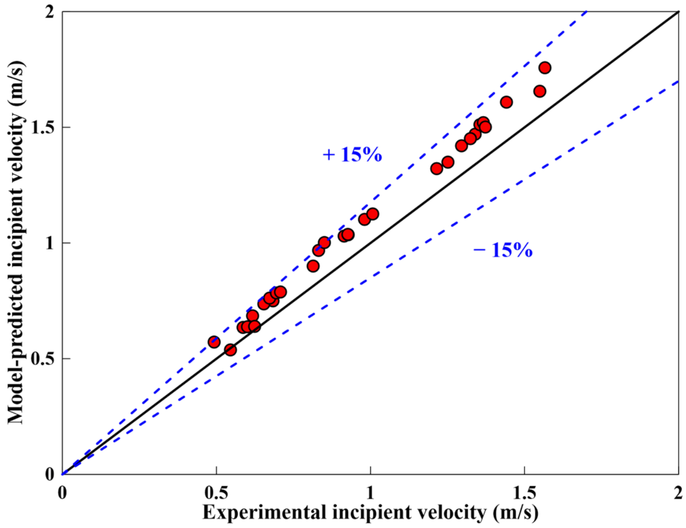

Figure 11. Calculation flow chart of incipient velocity for bed particles.

5. Conclusions

In this paper, the effects of the well's inclination angle, the cuttings size, and the different cuttings densities on the critical velocity of particle motion were analyzed experimentally, using a large-scale flow loop. Next, based on a stress analysis of the particles on the cuttings bed surface and of the boundary layer flow around the particles, an analytical formula for the surface shear force of the drilling fluid on the particles was derived and a critical velocity model was established. A verification was carried out and combined with the experimental results, as follows:

(1) The surface shear force can be calculated analytically from the angle of flow around the surface of the particles on the bed. The drag force can be approximately replaced by the surface shear force. The influence of the differential pressure resistance should be taken into account when calculating the drag force.
(2) By using the critical velocity, the critical displacement of the effective drilling fluid needed to maintain the erosion of the cuttings bed can be determined. The sinking of the cuttings bed has a greater impact on small particle sizes, while the effect of the pressure difference resistance on them is smaller.
(3) When the drilling fluid flows over the surface of the particles, the surface shear force plays a major driving role. If the particle size increases, the negative pressure formed by the vortex behind the particles also increases, which cannot be ignored.

Author Contributions: Methodology, K.S.; software, G.J. and Y.W.; validation, Z.X.; writing—original draft, K.S., Z.X. and G.J.; writing—review and editing, G.J. and Z.L. All authors have read and agreed to the published version of the manuscript.

Funding: This work was supported by the Marine Economy Development Foundation of Guangdong Province (GDNRC [2022]44) and the National Natural Science Foundation of China (Major Program, 51991361).

Data Availability Statement: Not applicable.

Conflicts of Interest: The authors declare no conflict of interest.

References

1. Yan, T.; Qu, J.Y.; Sun, X.F.; Li, W.; Chen, Y.; Hu, Q.B. A novel predictive model of drag coefficient and settling velocity of drill cuttings in non-Newtonian drilling fluids. *Pet. Sci.* **2021**, *18*, 1729–1738. [CrossRef]
2. Heydari, O.; Sahraei, E.; Skalle, P. Investigating the impact of drillpipe's rotation and eccentricity on cuttings transport phenomenon in various horizontal annuluses using computational fluid dynamics (CFD). *J. Pet. Sci. Eng.* **2017**, *156*, 801–813. [CrossRef]
3. Hu, Q.; Li, Y.; Sun, X.; Chen, M.; Bu, Q.; Gong, B. Integrating test device and method for creep failure and ultrasonic response of methane hydrate-bearing sediments. *Rev. Sci. Instrum.* **2023**, *94*, 025105. [CrossRef] [PubMed]
4. Zhang, F.; Miska, S.; Yu, M.; Ozbayoglu, E.; Takach, N.; Osgouei, R.E. Is well clean enough? A fast approach to estimate hole cleaning for directional drilling. In Proceedings of the Society of Petroleum Engineers—Coiled Tubing and Well Intervention Conference and Exhibition 2015, The Woodlands, TX, USA, 24–25 March 2015; pp. 603–618.
5. Mahmoud, H.; Hamza, A.; Nasser, M.S.; Hussein, I.A.; Ahmed, R.; Karami, H. Hole cleaning and drilling fluid sweeps in horizontal and deviated wells: Comprehensive review. *J. Pet. Sci. Eng.* **2020**, *186*, 106748. [CrossRef]
6. Alawami, M.; Bassam, M.; Gharbi, S.; Al Rubaii, M. A real-time indicator for the evaluation of hole cleaning efficiency. In Proceedings of the Society of Petroleum Engineers—SPE/IATMI Asia Pacific Oil and Gas Conference and Exhibition 2019, APOG 2019, Bali, Indonesia, 29–31 October 2019; pp. 29–31.
7. Naganawa, S.; Kudo, H.; Matsubuchi, H. Simulation study on influences of wellbore tortuosity on hole cleaning in extended-reach drilling. In Proceedings of the Society of Petroleum Engineers—Abu Dhabi International Petroleum Exhibition and Conference 2016, Denver, CO, USA, 5–6 May 2016.
8. Naganawa, S.; Sato, R.; Ishikawa, M. Cuttings-Transport Simulation Combined With Large-Scale-Flow-Loop Experimental Results and Logging-While-Drilling Data for Hole-Cleaning Evaluation in Directional Drilling. *SPE Drill. Complet.* **2017**, *32*, 194–207. [CrossRef]
9. Naganawa, S.; Nomura, T. Simulating transient behavior of cuttings transport over whole trajectory of extended-reach well. In Proceedings of the IADC/SPE Asia Pacific Drilling Technology Conference and Exhibition, Bangkok, Thailand, 13–15 November 2006; pp. 480–488. [CrossRef]
10. Yan, X.; Bu, Y.; Cheng, R. Research on numerical simulation of transient cuttings transport with foam fluid in horizontal section. *Drill. Fluid Complet. Fluid* **2011**, *28*, 24–28. [CrossRef]
11. Duan, M.; Miska, S.Z.; Yu, M.; Takach, N.E.; Zettner, R.M.A.C.M. Critical Conditions for Effective Sand-Sized Solids Transport in Horizontal and High-Angle Wells. *SPE Drill. Complet.* **2009**, *24*, 10. [CrossRef]
12. Huo, H.J.; Wang, R.H.; Ni, H.J.; Li, Y.X.; Tan, C.Y.; Xue, S. Study of critical annulus up-returning velocity of cuttings carried by supercritical CO2 in deviated well. *J. CO2 Util.* **2017**, *20*, 105–112. [CrossRef]
13. Qu, J.; Sun, X.; Yan, T.; Chen, Y.; Hu, Q. A novel prediction model for cuttings bed height in horizontal and deviated wells. *J. Nat. Gas Sci. Eng.* **2021**, *95*, 104192. [CrossRef]
14. Nguyen, D.; Rahman, S.S. Three-layer hydraulic program for effective cuttings transport and hole cleaning in highly deviated and horizontal wells. In Proceedings of the SPE/IADC Asia Pacific Drilling Technology, Kuala Lumpur, Malaysia, 9–11 September 1996; pp. 163–173. [CrossRef]
15. Kamp, A.M.; Rivero, M. Layer modeling for cuttings transport in highly inclined wellbores. In Proceedings of the Latin American and Caribbean Petroleum Engineering Conference, Caracas, Venezuela, 21–23 April 1999. [CrossRef]
16. Cheng, R.; Wang, R. A Three-Segment Hydraulic Model for Annular Cuttings Transport with Foam in Horizontal Drilling. *J. Hydrodyn.* **2008**, *20*, 67–73. [CrossRef]
17. Ozbayoglu, M.E.; Miska, S.Z.; Reed, T.; Takach, N. Using foam in horizontal well drilling: A cuttings transport modeling approach. *J. Pet. Sci. Eng.* **2005**, *46*, 267–282. [CrossRef]
18. Zhang, F.; Miska, S.; Yu, M.; Ozbayoglu, E.M.; Takach, N. Pressure Profile in Annulus: Solids Play a Significant Role. *J. Energy Resour. Technol. Trans. ASME* **2015**, *137*, 064502. [CrossRef]
19. Wang, Z.; Zhai, Y.; Hao, X.; Guo, X.; Sun, L. Numerical Simulation on Three Layer Dynamic Cutting Transport Model and Its Application on Extended Well Drilling. In Proceedings of the IADC/SPE Asia Pacific Drilling Technology Conference and Exhibition, Ho Chi Minh City, Vietnam, 1–3 November 2010; pp. 1–10. [CrossRef]
20. Clark, R.K.; Bickham, K.L. Mechanistic model for cuttings transport. In Proceedings of the SPE Annual Technical Conference and Exhibition, New Orleans, LA, USA, 25–28 September 1994; pp. 139–153. [CrossRef]
21. Ramadan, A.; Saasen, A.; Skalle, P. Application of the minimum transport velocity model for drag-reducing polymers. *J. Pet. Sci. Eng.* **2004**, *44*, 303–316. [CrossRef]
22. Mehmood, Y.; Shafqat, R.; Sarris, I.E.; Bilal, M.; Sajid, T.; Akhtar, T. Numerical Investigation of MWCNT and SWCNT Fluid Flow along with the Activation Energy Effects over Quartic Auto Catalytic Endothermic and Exothermic Chemical Reactions. *Mathematics* **2022**, *10*, 4636. [CrossRef]
23. Barkalov, K.; Lebedev, I.; Usova, M.; Romanova, D.; Ryazanov, D.; Strijhak, S. Optimization of Turbulence Model Parameters Using the Global Search Method Combined with Machine Learning. *Mathematics* **2022**, *10*, 2708. [CrossRef]
24. Li, S.; Chen, Z.; Li, W.; Yan, T.; Bi, F.; Tong, Y. An FE Simulation of the Fracture Characteristics of Blunt Rock Indenter Under Static and Harmonic Dynamic Loadings Using Cohesive Elements. *Rock Mech. Rock Eng.* **2023**, *56*, 2935–2947. [CrossRef]

25. Zhao, M.; Jha, A.; Liu, Q.; Millis, B.A.; Mahadevan-Jansen, A.; Lu, L.; Landman, B.A.; Tyska, M.J.; Huo, Y. Faster Mean-shift: GPU-accelerated clustering for cosine embedding-based cell segmentation and tracking. *Med. Image Anal.* **2021**, *71*, 102048. [CrossRef]
26. Li, Y.; Tang, B.; Geng, B.; Jiao, S. Fractional Order Fuzzy Dispersion Entropy and Its Application in Bearing Fault Diagnosis. *Fractal Fract.* **2022**, *6*, 544. [CrossRef]
27. Zhao, M.; Liu, Q.; Jha, A.; Deng, R.; Yao, T.; Mahadevan-Jansen, A.; Tyska, M.J.; Millis, B.A.; Huo, Y. *VoxelEmbed: 3D Instance Segmentation and Tracking with Voxel Embedding Based Deep Learning*; Springer International Publishing: Berlin/Heidelberg, Germany, 2021; Volume 12966, ISBN 9783030875886. [CrossRef]
28. Dodge, D.W.; Metzner, A.B. Turbulent flow of non-newtonian systems. *AIChE J.* **1959**, *5*, 189–204. [CrossRef]